

Ultrafast soft x-ray two-dimensional plasma imaging system based on gas electron multiplier detector with pixel readout

D. Pacella, G. Pizzicaroli, L. Gabellieri, and M. Leigheb

Associazione EURATOM-ENEA sulla Fusione, CR Frascati, 00044 Frascati, Rome, Italy

R. Bellazzini, A. Brez, G. Gariano, L. Latronico, N. Lumb, G. Spandre, M. M. Massai, and S. Reale

INFN-Pisa and University of Pisa, Pisa, Italy

(Received 29 August 2000; accepted for publication 11 November 2000)

In the present article a new diagnostic device in the soft x-ray range, for magnetic fusion plasmas, is proposed based on a gas electron multiplier detector with 2.5×2.5 cm active area, equipped with a true two-dimensional readout system. The readout printed circuit board, designed for these experiments, has 128 pads. Each pad is 2 mm square and covers a roughly circular area. The operational conditions of the detector are settled to work in the x-ray range 3–15 keV at very high counting rates, with a linear response up to 2 MHz/pixel. This limitation is due to the electronic dead time. Images of a wrench and two pinholes were done at rates of 2.5 MHz/pixel with a powerful x-ray laboratory source showing an excellent imaging capability. Finally preliminary measurements of x-ray emission from a magnetic fusion plasma were performed on the Frascati tokamak upgrade experiment. The system was able to image the plasma with a wide dynamic range (more than a factor of 100), with a sampling frequency of 20 kHz and with counting rates up to 4 MHz/pixel, following the changes of the x-ray plasma emissivity due to additional radio frequency heating. The spatial resolution and imaging properties of this detector have been studied in this work for conditions of high counting rates and high gain, with the detector fully illuminated by very intense x-ray sources (laboratory tube and tokamak plasma). © 2001 American Institute of Physics.

[DOI: 10.1063/1.1340026]

I. INTRODUCTION

In the present article a new diagnostic device in the soft x-ray range, for magnetic fusion plasmas, is proposed based on a gas electron multiplier (GEM) detector equipped with a true two-dimensional readout system. By means of a pinhole camera configuration, the plasma has been imaged on the detector with a very high sampling rate (tens of kHz). A readout board with 128 pixels has been designed for this purpose and coupled to a GEM detector with 2.5×2.5 cm active area. The system has been set up in our laboratory and then successfully tested with the plasma of the Frascati Tokamak Upgrade (FTU).

The GEM device, with a selectable sensitivity in the soft x ray, can be used to image plasmas at very high frequency, to study spatial distribution of x-ray emission, during many plasma processes, such as instabilities, effects of additional heating, turbulence and so on.

The features of the GEM detectors will be briefly summarized in Sec. II; electronics, acquisition system and laboratory tests will be discussed in Sec. III. The general layout of the proposed diagnostic will be shown in Sec. IV, together with estimations of the plasma emissivity in the range of interest. Finally, in Sec. V the preliminary results on the FTU tokamak will be presented.

II. GAS ELECTRON MULTIPLIER DETECTOR

A. General features

Microelectronics and advanced printed circuit technology opened the way to a new generation of gas detectors. Examples of these new devices are micro-strip gas chambers and micro-gap chambers based on microelectronic techniques (thin film photolithography) and gas electron multipliers (GEM), well detectors, and groove detectors based on advanced printed circuit board (PCB) techniques.¹

The submillimeter dimensions of the amplification cells of these devices permit the main operational characteristics: high spatial resolution and high counting rate.

The GEM have been developed at CERN by Sauli² and their principle of operation is shown in Fig. 1(a).³ The detector consists of a ‘‘drift’’ and a ‘‘transfer’’ gas volume, separated by a composite mesh acting as an amplifier (‘‘gem foil’’). The drift region is defined by the cathode and the upper face of the gem foil, while the transfer region between its lower face and the readout PCB. The gem foil is a thin polymer foil, metal clad on both sides and pierced by a high density of narrow holes (typically 70 μm at 140 μm pitch). Potential differences applied between the cathode and the readout PCB and to the gem foil generate the field structure as shown in Fig. 1(b). Primary electrons, produced by the photoelectron following the absorption of the x-ray photon in

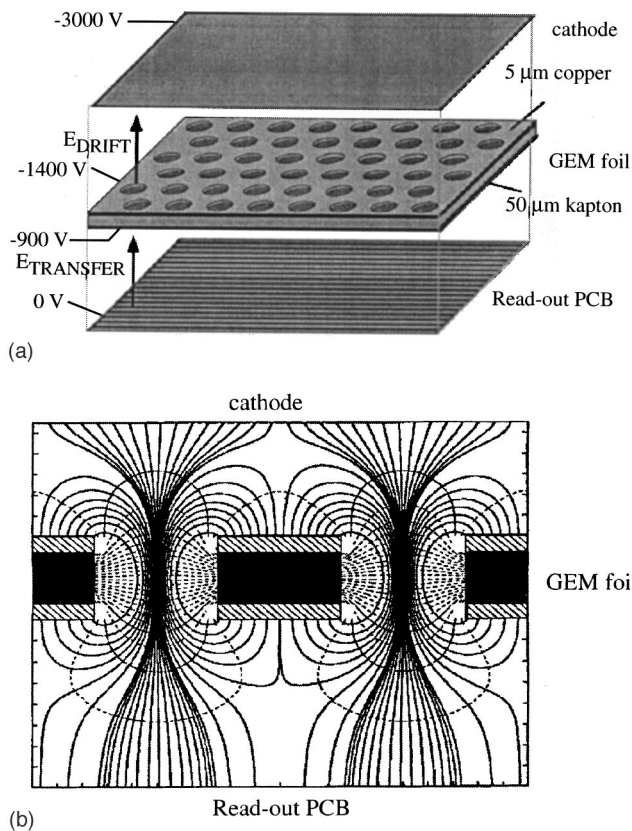


FIG. 1. Principle of working of the GEM detector. (a) Planes, electrodes and polarizations, (b) cross section of the electric field structure.

the upper part of the chamber, drift into the holes where the multiplication occurs. Electrons are then collected on the lower printed board (PCB). These detectors have an important feature: electron multiplication and readout functions are separated. Consequently, the readout board can be designed with any geometry and optimized or adapted for the specific purposes of allowing for a flexible readout, high counting rate, large gain range and good spatial resolution.

The spatial resolution and imaging properties of this detector have been studied in this work for conditions of high counting rates and high gain, with the detector fully illuminated by very intense x-ray sources (laboratory tube and tokamak plasma).

B. Detector and readout

In our detector, the gem structure is a kapton foil 50 μm thick, with a 4-μm-thick copper coating on each side. A chemical etching process⁴ produces holes with a double-conical shape, which are wider in the metal layers than in the kapton. The diameter in the copper surfaces is 70 μm. The holes have a triangular pattern with a distance between the centers of 90 μm to maximize the number of openings of the GEM surface. The cathode is an aluminized mylar foil. The drift region is 4 mm high and the transfer region 1.3 mm. The collection plane is a printed circuit board with 128 square pads. Each pad is 2 mm square and covers a roughly circular area (Fig. 2). The efficiency of collection of the primary electrons into the holes (gem transparency) is maximized with the geometric pattern above described and the

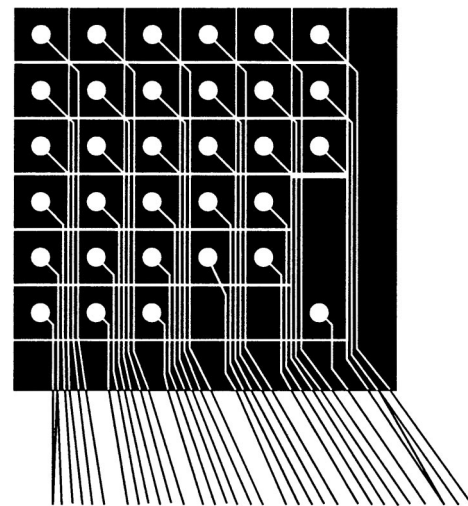


FIG. 2. One fourth (fourth quadrant) of the printed circuit board with the central readout of the GEM detector with the pixels (32 of 128) and their relative connections.

optimized ratio between the electric field of the drift gap and of the GEM foil. The squeezing of these two electric fields inside the hole produces a field of the order of 10⁵ V/cm [see Fig. 1(a)]. If the field in the transfer region is greater than 6 kV/cm, most of the exiting electrons are collected on the readout plane and generate a short current pulse (20 ns) that can be detected by a fast electronics. Each pixel is connected to a fast charge preamplifier (LABEN 5231), an amplifier (LABEN 5185), a low threshold discriminator (LeCroy 4608C) and a latched scaler CAMAC (LeCroy 8590). Electronic boards with charge sensitive preamplifiers are directly mounted on the detector case to minimize the parasitic capacitance and reduce the sources of noise. The fast, low noise electronics coupled to the discriminators and asynchronous scalers ensure high quality data resulting in only statistical noise.

Two x-ray sources have been used in the laboratory tests: a weak radioactive source of Fe⁵⁵ (about 10 mCi) emitting at 5.9 keV and a powerful (10 kW) x-ray source (Philips TW 1730), whose electronic tube, with tungsten cathode, operates in the range 20–60 kV voltage range with 5–60 mA of current. Tests on the GEM detector have been carried out at 20 kV with 5–30 mA of current. The x-ray tube source is spatially uniform with area 0.5×1 cm, and emits a continuum spectrum from 2 to 20 keV. In the laboratory tests the x-ray tube source was placed 55 cm from the GEM detector and, because of the air transmission, the minimum energy of the x-ray photons arriving to the detector was about 5 keV.

The gas mixture of the GEM detector used in this experiment is Ar 66% and DiMethylEther 33%. The operational voltages of the chamber are determined by two requirements: high gain to detect photons in the 3–15 keV range and very high counting rates. Consequently, the electron signal corresponding to each converted photon has to be as low as possible to minimize the charge produced in the detector but higher than the detector noise threshold.

Since the electronic noise due to preamplifier and amplifier is very low (4–7 mV rms), we used a discriminator threshold of 30 mV. The gain of the GEM, in the interval

1000–2500, is fixed to have the peak of Fe^{55} (5.9 keV) at 75 mV for lower gain or at 200 mV for higher gain. This depended on the kind of source (x-ray tube, radioactive source or plasma) and the purpose of the measurements (counting mode or spectral analysis). Drift and transfer electric fields are quite high to have a good match between large gains and high transparency of the GEM ($E_d = 5.5$ kV/cm) and a fast electron transfer to the readout ($E_i = 7.5$ kV/cm). These fields are obtained with the readout board grounded and three high voltage power supplies, with negative polarity, for the two faces of the GEM and the cathode (Fig. 1). The resulting potential differences are, in absolute values, $\Delta V_i = 900$ V for the transfer gap, $\Delta V_{\text{gem}} = 480$ V for the gem foil and $\Delta V_d = 1620$ V for the drift gap. With these parameters, electron signals on the pixels with Fe^{55} are in the range 30–130 mV, with a time duration of 50 ns full width at half maximum. Since the electronic front end (preamplifiers and amplifiers) is linear, the pulse amplitude of the final signal is proportional to the total number of electrons collected on the pixel. This factor has been measured and it is approximately $1 \mu\text{V}/e$. Since the photons at 6 keV (Fe^{55}) produce about 200 primary electrons, the gain of the GEM has been easily estimated.

III. LABORATORY TESTS

A. Detector response at high fluxes

The whole system, detector and 128 independent electronic channels has been tested in the laboratory to study the imaging properties at very high counting rate (up to 6 MHz/pixel).

To obtain an x-ray image, absolute counts of 128 channels have to be compared. Therefore, the counting rate of each pixel has to be insensitive to fine adjustment of the discrimination threshold or small differences in electronic gain (condition of counting plateau). Since the detector is working in a proportional regime, the amplitude of each pulse is proportional to the energy of the absorbed photon. In our condition, the peak of Fe^{55} (5.9 keV) corresponds to a pulse height of 75 mV. Since the threshold (30 mV corresponding to 2.4 keV) is much lower than the minimum energy of the photons arriving to the detector (about 4 keV), the required condition of counting plateau is satisfied. This condition also prevents the systematic error due to the base line shift of the amplifiers at very high counting rates, as observed on the oscilloscope at rates of the order of a few Mhz per pixel which produces an increase of the base line. Since the signals are negative, this corresponds to a raising of the absolute value of the effective threshold. Since the change can be up to 30%, the threshold is low enough that the minimum energy of the photons and counting is not affected. The same condition is matched on the tokamak FTU where the continuum spectrum emitted by the plasma is filtered, at low energy, by two windows (Be $100 \mu\text{m}$ and mylar $50 \mu\text{m}$) and 10 cm of air. In Fig. 3 the counts of the GEM detector as a function of the discriminator threshold are plotted using both the x-ray tube (20 kV, 5 mA) and the Fe^{55} source as x-ray generators. The relation between the pulse amplitude and the photon energy has been obtained by

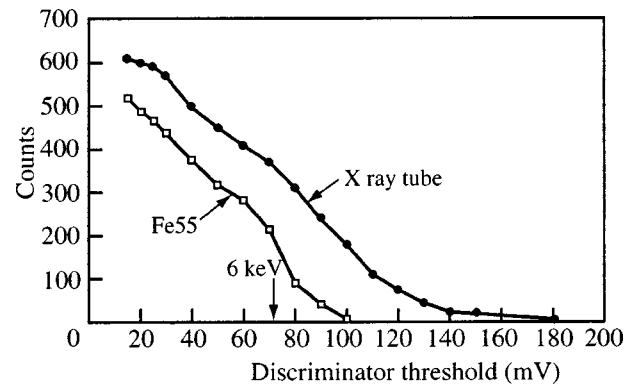


FIG. 3. Counts as function of the discriminator threshold with Fe^{55} source and with x-ray electronic tube. An arrow indicates the correspondence between threshold (in mV) and x-ray energy.

means of the spectrum of Fe^{55} . The curve obtained with the radioactive source does not show the counting plateau because of the “escape peak” of the Ar [see spectrum in Fig. 13(b)], falling at 2.8 keV, comparable to the threshold. In the case with the x-ray tube, since most of the photons have higher energy than Fe^{55} , the escape peak is almost entirely beyond the threshold and the plateau is approached.

As a third step, the linearity of the GEM response has been tested at extremely high flux rates. The current in the upper face of the GEM (where part of the ions produced in the avalanche in the hole are collected) and the counts per pixel are plotted in Figs. 4(a) and 4(b) for different values of the x-ray tube current. The source has been screened by a foil of Al $200 \mu\text{m}$ thick to limit the x-ray flux onto the detector [Fig. 4(a)]. These curves show an excellent linearity up to 2 MHz/pixel. Since the current measured on the upper face of the GEM (I_{GEM}) is proportional to the detected photons, we can conclude that the response is linear [Figs. 4(a) and 4(b)] over all the measured range. On the contrary, the number of photons counted by the electrons is linear up to 2 MHz/pixel [Fig. 4(a)] and saturates at higher values [Fig. 4(b)]. This lack of linearity is due to the dead time of the electronics. Experimental points are indeed well fitted (continuous curve) with a dead time of about 170 ns. It can be concluded that in our experiment setup the limit is given by the electronics, being higher than the limit of the chamber. The maximum number of counted photons in this configuration is 4 MHz/pixel (corresponding to 10^6 ph/s mm^2). Since the time duration of the electronic signals can be reduced, in the next experiments, the counting rates will be increased.

B. Imaging properties at high fluxes

Once the parameters of the detector have been set up to allow the highest counting rates, measurements were performed in the laboratory to study the imaging properties in these conditions (e.g., spatial resolution, cross talk of adjacent pixels, dynamic of the pattern, sharpness of the edge between light and shadow, etc.).

In the preliminary test, the uniformity of the detector response has been checked, since the x-ray source is very uniform. The statistical distribution of the pixel counts is

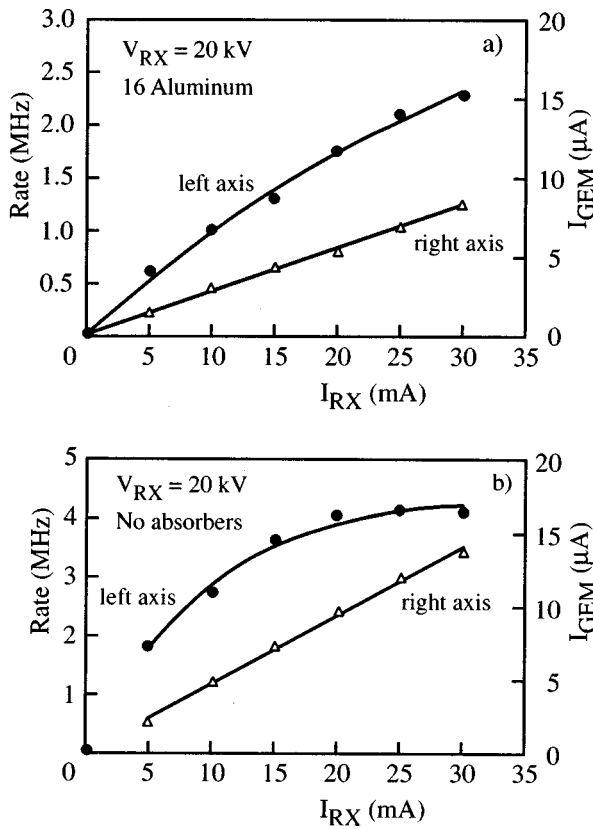


FIG. 4. Current measured on the top face of the GEM (right ordinate) and counting rates (left ordinate) on 1 pixel for different x-ray tube intensities. (a) With 200 μm of aluminum as a filter, (b) without any absorber. Continuous line for the counts is a fit taking care of the electronic dead time (170 ns).

Gaussian like with a standard deviation of about 5% of the mean value.

The first measurement has been done with a lead shield 2 cm from the detector and the x-ray source 55 cm distant. The shield had two pinholes of diameter, respectively, 1 and 1.3 mm. The image is plotted in Fig. 5. The smallest pinhole is quite well centered on a pixel, whose counts are 75% of the total with only one pixel significantly illuminated. On the contrary, the largest pinhole illuminates four adjacent pixels. The total counts of the two pinholes are proportional to their respective area. The background counts in the rest of the chamber are less than 2% of the peak of the pinholes and result from fluorescence of the lead shield.

In the second measurement, the smallest pinhole has been shifted 1 mm in a few steps. In the intermediate positions the interchange of the two close pixels is observed. Total counts in all the steps vary by less than 5%. Within a few percent, each photon is counted only once (no multiple events) and no cross talk is observed, as expected because the dimensions of the pixels are greater than the transverse spread of the electrons.

The third measurement is a shadowgraph of a wrench (Fig. 6), placed close to the detector. Also in this case the x-ray detected flux is of the order of 2 MHz/pixel. In the representation the area of the square related to each pixel is proportional to the counts. The edge between light and

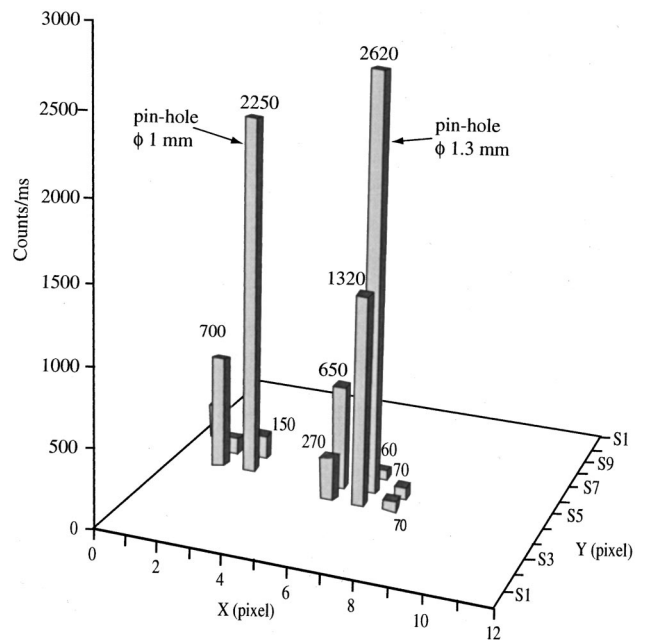


FIG. 5. Image with the x-ray tube of a lead shield with two pinholes, placed close to the detector. The diameters of the two pinholes are 1 and 1.3 mm. The background is less than 20 counts/ms.

shadow is well defined and the ratio (contrast) between two adjacent pixels at the edge is about 20.

These tests have revealed excellent imaging properties of this detector at very high rates (2.6 MHz/pixel). The shape of the wrench is recognizable, even with a restricted number of pixels.

IV. LAYOUT OF THE IMAGING SYSTEM AT FTU

FTU is a compact, high field tokamak^{5,6} with major radius $R=0.935$ m, minor radius $a=0.3$ m, toroidal field $B_t \leq 8$ T and plasma current $I_p \leq 1.6$ MA, with the ability to

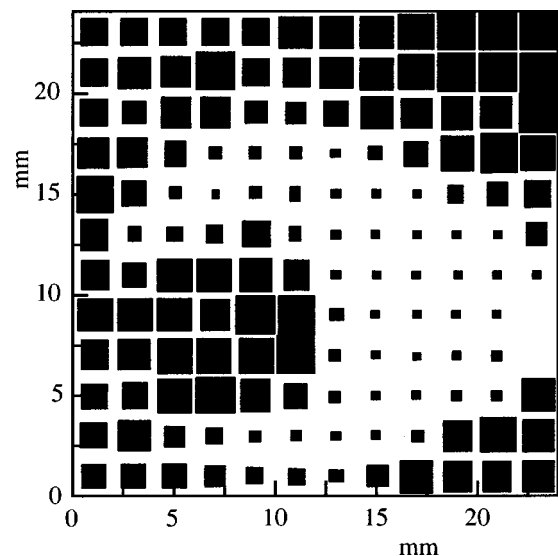


FIG. 6. Image of a stainless steel wrench placed close to the detector, at very high counting rates (about 2 MHz/pixel). In the representation the area of the square related to each pixel is proportional to the counts.

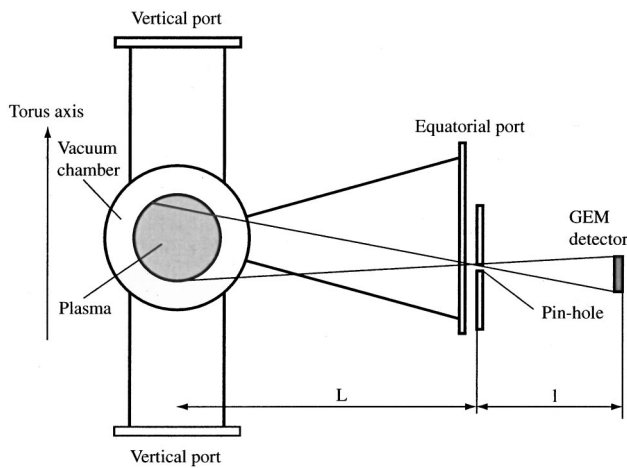


FIG. 7. Schematic view of plasma cross section, port, pinhole and GEM detector for the FTU tokamak.

operate over a wide range of densities ($0.3\text{--}3.0 \times 10^{20} \text{ m}^{-3}$). The plasma discharges last about 1.6 s with a current flattop of 1.2 s.

The total number of photons emitted by the plasma reaching the detector is

$$N = \int_V \epsilon(x, y, z) \Delta\Omega dx dy dz,$$

where ϵ is the emissivity as a function of the spatial coordinates and $\Delta\Omega$ is the solid angle of the detector viewed by a point in the plasma (Fig. 7). Due to the tokamak axisymmetry and the perpendicular observation of the plasma, only one-dimensional images can be done as a function of the minor radius. Taking into account the conversion efficiency $\alpha(E)$ of the detector (window transmission and gas absorption) as function of the photon energy E , we can estimate the number of detected photons N_E in each pad i, j (pixel) of the readout board, with energy greater or equal than E

$$N_E(i, j) = \int_{V_{ij}} \Delta\Omega(i, j) dx dy dz \int_E^\infty dE \alpha_E \epsilon_E(x, y, z, E),$$

where the spatial integration is performed over the plasma volume V_{ij} whose image is formed on the pad i, j .

The preliminary measurements, discussed in the following, have been performed with a rectangular slit 20 mm wide (b_1) horizontal and 2 mm high (vertical) (b_2) placed on the equatorial port at roughly 200 cm from the center of the plasma.

Since the FTU tokamak has ports far from the plasma ($L \gg a$), the expression for solid angle can be approximated as a constant and moved out of the integral

$$\Delta\Omega \approx \frac{b_1 b_2}{L^2} \quad N \approx \Delta\Omega \int_V \epsilon dx dy dz.$$

The optical resolution of the image due to the slit, 2 mm high, is comparable with the spatial resolution of the detector.

With a rotating crystal spectrometer,⁷ brightness (line integrated emissivity) along a central line of sight was measured⁸ and shown in Fig. 11, expressed in wavelength

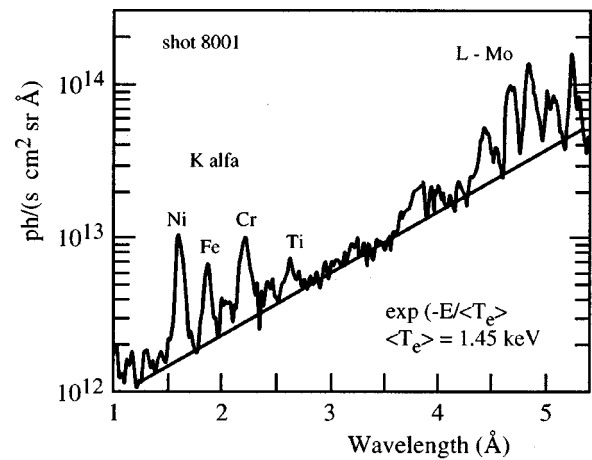


FIG. 8. X-ray spectrum for an ohmic plasma of FTU tokamak.

(Å), for a typical ohmic plasma (central electron temperature of about 2 keV and density 10^{14} cm^{-3}). The spectral distribution is due to a continuum contribution, well fitted by an exponential decay $\exp(-E/kT)$, and by line emissions (quasi-continuum of recombination is negligible in this range). In particular, there are strong L -shell emissions of molybdenum⁷ (transition energy 2–3 keV) and the K -shell emissions of Ni, Fe, Cr (4–7 keV). Since the x-ray range measured at the FTU with this GEM detector is 4–15 keV (0.8–3 Å), we can estimate, from the spectrum of Fig. 8, the averaged emissivity $\bar{\epsilon} = 10^{11} \text{ (ph/s cm}^3 \text{ sr)}$ in this range. Since the volume of the plasma seen by the detector through the slit is roughly 10^3 cm^3 , the total number of photons arriving at the chamber is about 10^9 s^{-1} .

Taking into account the absorption efficiency of the gas (Ar) of the GEM chamber, we can estimate a detected photon flux of 1 MHz/pixel equivalent to $2.5 \times 10^5 \text{ ph/s mm}^2$. Since the counting rate limit is much higher, as shown in Sec. III, the detector can also measure more intense x-ray emitting plasmas, as in the case of additional heating with radio frequency power. In the configuration previously described, we can select two different sampling frequencies of the scalars: one lower at 1 kHz and one higher at 20 kHz. In this second case it is necessary to work in conditions of very high flux rates ($>1 \text{ MHz/pixel}$) to reduce the statistic fluctuations of the sampling. Moreover, it is possible to settle the minimum energy of the detected photon, adjusting the low threshold of the discriminators. Using double threshold discriminators it should be possible to have image in a preset range of energy.

V. PRELIMINARY RESULTS ON THE FTU TOKAMAK

Since a tokamak is a harsh environment, both for electrical noise and for radiation (neutrons, gamma rays), a preliminary check of the noise on the system was performed. In a standard plasma discharge, with the detector not illuminated, the rate increased to 300–400 Hz in the plasma start-up phase and was around 100 Hz in the steady state.

When the GEM detector is exposed to the plasma, the counting rate for central lines of sight can vary from 100 kHz

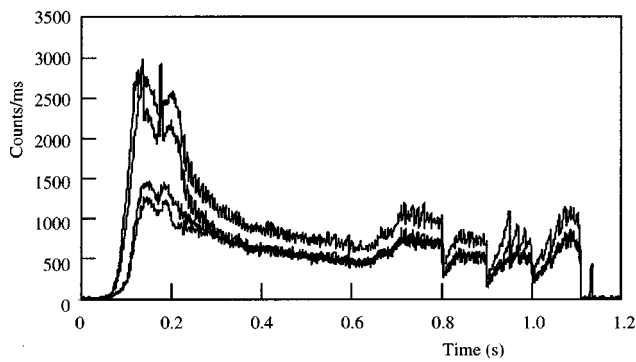


FIG. 9. Signals from 4 pixels of the GEM detector with a central line of sight and for an ohmic plasma.

to 6 MHz, depending on the plasma conditions, as shown in the following. The signal to noise ratio is therefore in the range $10^3 - 10^5$.

The new diagnostic system was mounted on the FTU in a temporary and not optimized arrangement just to have the preliminary tests on plasma and to check the performance and potentiality of the GEM detectors as diagnostic system. The optical view of the detector is limited to roughly one third of the minor radius. To view the x-ray emissions as functions of the radius, the device was tilted off axis.

Time histories of 4 pixels are shown in Fig. 9 for shot 18 608. Since the GEM detector is aligned along the central line of sight, the pixels show just small differences with the spatial position (in the start-up phase the difference is a bit higher because the soft x-emissivity radial profile is very peaked at the center). The signals follow the line evolutions of the soft x-ray emissions. For example, the drops at $t = 0.8$, $t = 0.9$, and $t = 1.0$ s are caused by sudden increases of

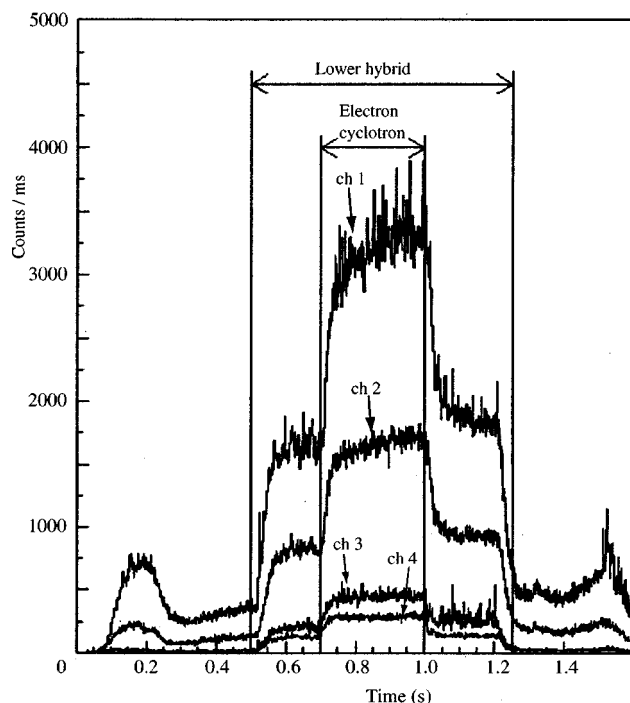


FIG. 10. Signals from 4 pixels of the GEM detector aligned off axis for a plasma heated with radio frequency power (LH and ECRH) from ch 1 more central to ch 4 at half radius.

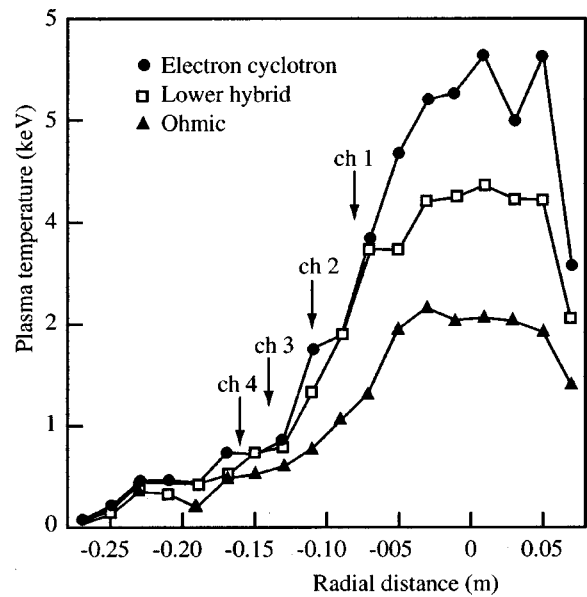


FIG. 11. Electron temperature radial profiles from Thomson scattering for the shot of Fig. 13. The lines of sight of the pixels of Fig. 13 are shown.

density due to D_2 multiple pellet injections. The counting rates vary from 1 (flattop) to 3 (start-up phase) MHz/pixels.

The system has been tilted to investigate the intermediate radial position ($8 < r < 16$ cm) where the largest gradients occur. In this position the signals of the pixels (ch 3,4 of Fig. 10) that view the outer region are very low in the ohmic phase and grow when plasma is heated by lower hybrid (LH) and electron cyclotron heating (ECRH).^{9,10} The radial positions of the plasma viewed by the pixels ch 1,2,3,4 (Fig. 10) are indicated in Fig. 11 together with the electron temperature radial profiles¹¹ at three different times (ohmic, LH, LH + ECRH), measured by means of Thomson scattering. Signals with higher sampling rate (20 kHz) are shown in Fig. 12. The spectral distribution of the photons emitted by the plasma and detected by the chamber is shown in Fig. 13 for

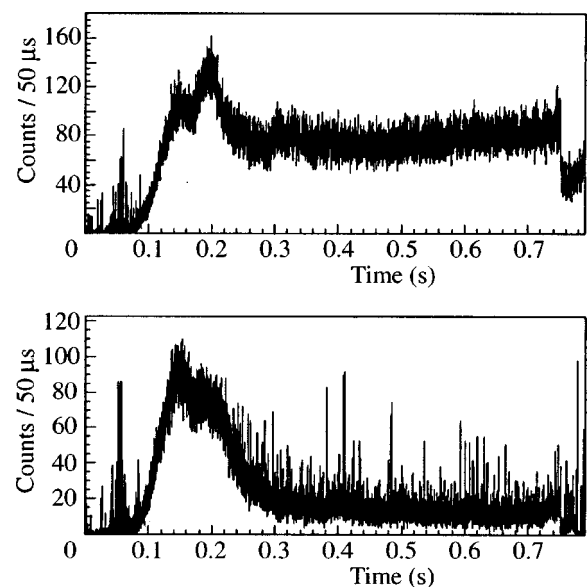


FIG. 12. Examples of fast acquisition with 20 kHz of sampling frequency for two ohmic shots.

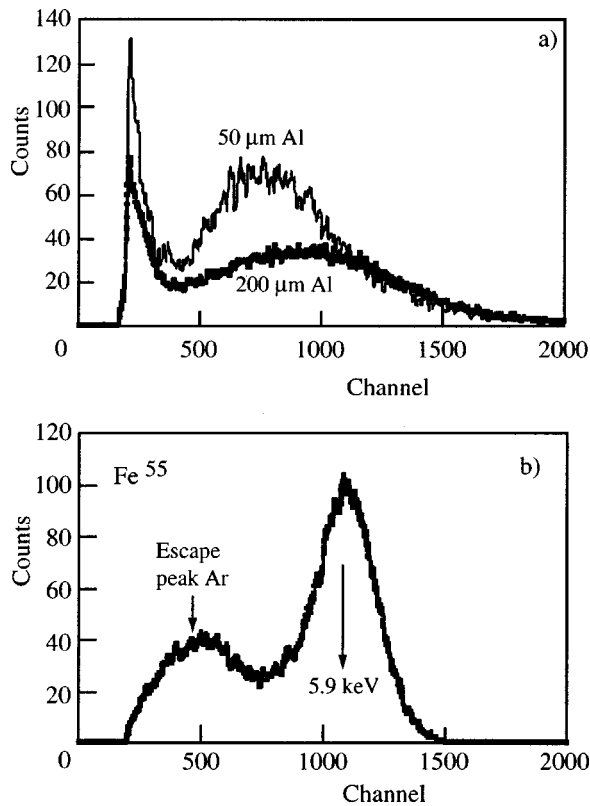


FIG. 13. (a) Spectra of ohmic plasma obtained from 1 pixel of the GEM detector with 200 and 50 μm of aluminum as absorber, (b) spectrum of the same pixel with a Fe^{55} source for calibration in energy.

a pixel looking at the center of the plasma and integrated in time during the shot. The two spectra are obtained with two different absorbers: 200 μm of aluminum in one case and 50 μm in the other. The calibration in energy of the abscissa was done using the spectrum of Fe^{55} [Fig. 13(b)]. The energy resolution is poorer because the measurement was performed on a single pixel and the events, whose charge is also collected by adjacent pixels, are underestimated in energy. Finally, in Fig. 14 the top, central and bottom pixels are plotted in logarithmic scale for three similar shots where the device has been tilted to cover most of the x-ray emitting plasma ($0 < r < 20$ cm). The signal level varies over almost two orders of magnitude (for the most peripheral signals, sampling frequency was reduced to 200 Hz), demonstrating the high dynamic range of this device.

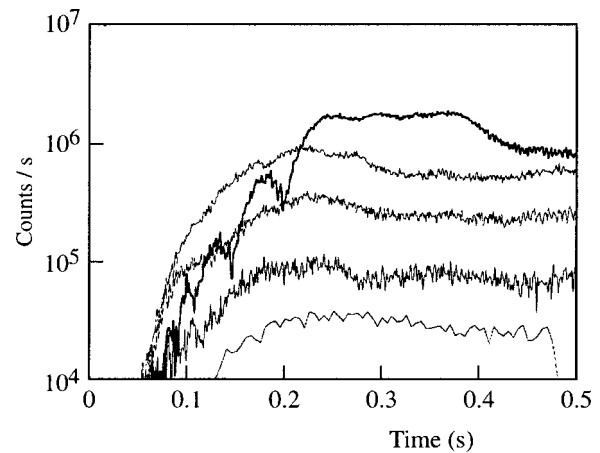


FIG. 14. Signals from 3 pixels (top, intermediate and bottom) for three similar plasma discharges with GEM detector tilted to cover the radial range from 0 to 20 cm.

ACKNOWLEDGMENTS

The authors would like to acknowledge F. Sauli for the precious and fruitful discussions about these detectors. The authors would also like to acknowledge the assistance of A. Gandi, R. De Oliveira, and L. Mastrostefano of the CERN advanced printed circuit workshop, for their skill and experience in the production of GEM electrode structures.

- ¹F. Sauli, Nucl. Instrum. Methods Phys. Res. A **419**, 189 (1998).
- ²F. Sauli, Nucl. Instrum. Methods Phys. Res. A **386**, 531 (1997).
- ³R. Bellazzini, A. Brez, G. Gariano, L. Latronico, N. Lumb, G. Spandre, M. M. Massai, R. Raffo, and M. A. Spezziga, Nucl. Instrum. Methods Phys. Res. A **419**, 429 (1998).
- ⁴A. Gandi *et al.*, Manufacturing procedures for the gas electron multiplier, in preparation at CERN, 1997.
- ⁵R. Andreani, Fusion Eng. Des. **22**, 129 (1993).
- ⁶F. Alladio *et al.*, Plasma Phys. Controlled Fusion **36**, 12B (1994).
- ⁷K. B. Fournier, W. H. Goldstein, D. Pacella, R. Bartiromo, M. Finkenthal, and M. May, Phys. Rev. E **53**, 1084 (1996).
- ⁸D. Pacella, M. Mattioli, R. Bartiromo, K. B. Fournier, and M. Finkenthal, Proceedings of the 23rd EPS Conference on Controlled Fusion and Plasma Physics, Kiev, Ukraine, 1996.
- ⁹D. Pacella, K. B. Fournier, M. Zerbin, M. Finkenthal, M. Mattioli, M. J. May, and W. H. Goldstein, Phys. Rev. E **61**, 5701 (2000).
- ¹⁰M. Zerbin, P. Buratti, O. Tudisco, G. Giruzzi, A. Bruschi, S. Cyrant, G. Granucci, A. Simonetto, C. Sozzi, F. Gandini, D. Pacella, K. B. Fournier, and M. Finkenthal, Rev. Sci. Instrum. **70**, 1007 (1999).
- ¹¹F. Orsitto, A. Brusadin, E. Giovannozzi, D. Santi, R. Bartiromo, and P. Pizzolati, Appl. Opt. **34**, 2712 (1995).